Supporting Information

PtIr Nanowires for Efficient Electrochemical Ammonia Oxidation

Chun Song[a], Jinjie Fang[a], Chengjin Chen[a], Xuejiang Zhang[a], Yufeng Zhang[a], Wei Zhu*[a], and Zhongbin Zhuang*[a]

Experimental Section

1. Reagents

Platinum(II) acetylacetonate ($Pt(acac)_2$, 98%, Alfa Aesar), iridium (III) acetylacetonate ($Ir(acac)_3$, 97%, Alfa Aesar), chloroplatinic acid (H_2PtCl_4, 99%, Aladdin), iridium(III) chloride hydrate ($IrCl_3 \cdot xH_2O$, 99%, Sigma-Aldrich), tungsten hexacarbonyl ($W(CO)_6$), oleylamine (OAm, 80-90%, Aladdin), cyclohexane (>99.5%, Sinopharm), dodecyl dimethyl ammonium bromide (DDAB, 99%, Sinopharm Chemical Reagent Co. Ltd), cetyltrimethylammonium bromide (CTAB, 99%, Sinopharm Chemical Reagent Co. Ltd), cetyltrimethylammonium chloride (CTAC, 98%, Sinopharm Chemical Reagent Co. Ltd), aqueous ammonia ($NH_3 \cdot H_2O$, 25-28 wt.%, Aladdin), Nafion solution (5%, Dupont), and potassium hydroxide (KOH, 99.99%, Aladdin) were used as received without further purification.

2. Synthesis of the PtIr NWs and control samples

Synthesis of the PtIr NWs. 100 mg of DDAB and 60 mg of hexacarbonyl tungsten were added into a 10 mL flask. $W(CO)_6$ was introduced as a structure-directing agent to promote anisotropic growth of ultrathin PtIr nanowires. Then, 3 mL of OAm was added, and the mixture was stirred at 80°C to form a homogeneous solution. Next, 10 mg of $Pt(acac)_2$ and 13 mg of $Ir(acac)_3$ were added to the above solution. The mixture was stirred at 80°C to form a homogeneous solution. The flask was then transferred to an oil bath at 170°C, and the reaction was allowed to proceed for 4 h under magnetic stirring. After the reaction, the solution was transferred to a centrifuge tube, and ethanol was added for centrifugation. The products were collected by centrifugation and washed four times with ethanol. Finally, the product was redispersed in cyclohexane.

Synthesis of the PtIr NPs. 40 mg of carbon powder (Vulcan XC-72R), chloroplatinic acid (100 mg mL^{-1}, 123 μL), and iridium chloride (5 mg mL^{-1}, 636 μL) were mixed and sonicated for 2 h. Then it was rotary evaporated at 60°C. The obtained powder was then dried overnight in an oven, ground, and calcined at 700°C under a H_2 atmosphere for 1 h using a tube furnace to obtain the PtIr NPs.

3. Loading Nanocrystals on Carbon Supports

Carbon powder pretreatment. Carbon powder (20 mg) was pretreated in a tube furnace under flowing air (100 mL min^{-1}) at 500 °C for 5 h. Then, it was added to a 125 mL flask, and the mixture was stirred overnight. After stirring, filter the liquid by suction, transfer it to a clean Petri dish, and place it in a 50°C oven overnight.

Loading the PtIr NWs on high surface area carbon. Treated high surface area carbon was first dispersed in cyclohexane and uniformly dispersed under ultrasonic assistance. Subsequently, the synthesized platinum-iridium nanowire dispersion was added dropwise. The mixed solution continued to undergo ultrasonic treatment for 30 minutes, followed by stirring for 120 minutes. The resulting carbon-supported catalyst was collected by filtration and dried in an oven. It was then calcined in an air atmosphere at 200°C for 5 hours to remove the surfactant. The precise loading of iridium (Ir) and platinum (Pt) in the catalyst was determined by inductively coupled plasma optical emission spectroscopy (ICP-OES).

4. Characterizations

The transmission electron microscopy (TEM) images were captured using a JEOL JEM-1230 transmission electron microscope, and the high-resolution TEM (HRTEM) images were acquired with a JEOL JEM-2010F transmission electron microscope. Elemental mapping analyses via energy-dispersive X-ray spectrometry (EDS) were conducted using a Thermo Fisher Scientific Talos F200X. X-ray photoelectron spectroscopy (XPS) measurements were performed on a Thermo Fisher ESCALAB 250 Xi XPS system, utilizing a monochromatic Al Kα X-ray source. X-ray powder diffraction (XRD) patterns were obtained using a Rigaku D/Max 2500 VB2+/PC X-ray powder diffractometer equipped with Cu Kα radiation (λ = 0.154 nm), at a scan rate of 5° min^{-1}. The metal contents of the prepared catalysts were determined using inductively coupled plasma optical emission spectroscopy (ICP-OES, Optima 7300 DV, Perkin Elmer). The ultraviolet photoelectron spectroscopy (UPS) was conducted on a Thermo SCIENTIFIC Nexsa equipped with Thermo Avantage v 59921.

5. Electrochemical characterizations

Electrochemical measurements were performed using an electrochemical workstation (Princeton Applied Research, V3) with a standard three-electrode system at room temperature. The reference electrode is a mercury/mercury oxide (Hg/HgO) electrode, and the counter electrode was a carbon rod. The catalyst ink was prepared by dispersing 1 mg of catalyst powder in 1 mL of a mixed solution containing ethanol (800 μL), water (190 μL), and Nafion (5 wt%, 10 μL). A 10 μL aliquot of the catalyst ink was then deposited onto a glassy carbon electrode (5 mm in diameter, PINE instruments) to serve as the working electrode. Deionized water (18.2 MΩ·cm) was used in all electrochemical experiments. All potentials reported in this work were converted to the reversible hydrogen electrode (RHE) scale. The solution resistances, measured by AC impedance spectroscopy, were corrected for the polarization curves.

In situ electrochemical attenuated total reflection surface-enhanced infrared absorption spectroscopy (ATR-SEIRAS) measurements were carried out using a Nicolet iS50 FT-IR spectrometer equipped with an MCT detector cooled with liquid nitrogen and a PIKE VeeMAX III variable angle ATR sampling accessory. The spectral resolution was set to 4 cm^{-1} and 64 interferograms were coadded for each spectrum. The spectra are given in absorption units defined as $A=-\log(R/R_0)$, where R and R_0 represent the reflected IWR intensities corresponding to the sample and reference-single beam spectrum, respectively. A 60° Si face-angled crystal was used as the reflection element. The ultrathin Au film was deposited chemically in it for IR-signal enhancement and conduction of electrons. The electrocatalyst was dropped onto the Au film to serve as a working electrode for SEIRAS experiments with a loading of 0.05 mg cm^{-2}. The catalysts fully covered the Au film. A carbon rod and an Ag/AgCl electrode were used as the counter and reference electrode in all tests, respectively. The chronopotentiometry method was used in this experiment at different potentials (0.1 to 0.8 V vs RHE without iR correction). The SEIRAS spectra were collected during the chronopotentiometry test. The reference spectra were collected at 0 V.

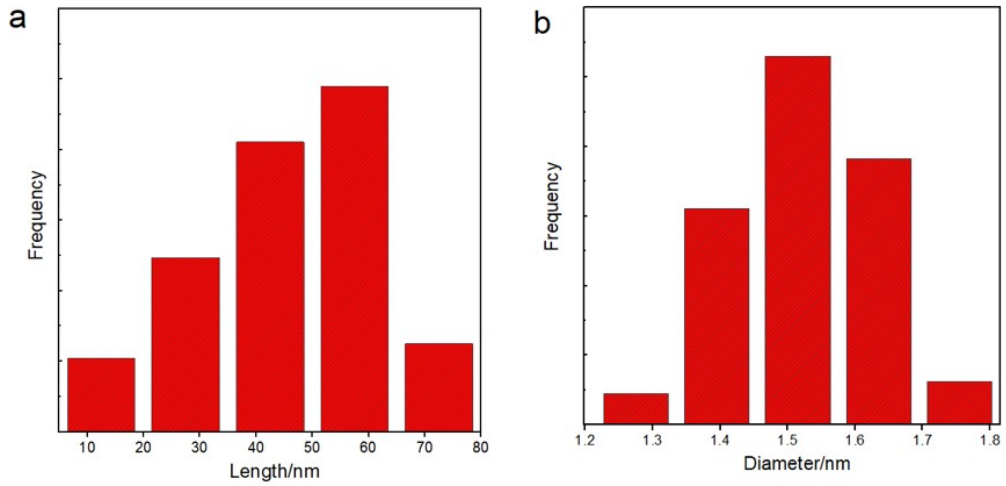

Figure S1. Size distribution histogram of the PtIr NWs derived from TEM images. (a) length. (b) diameter.

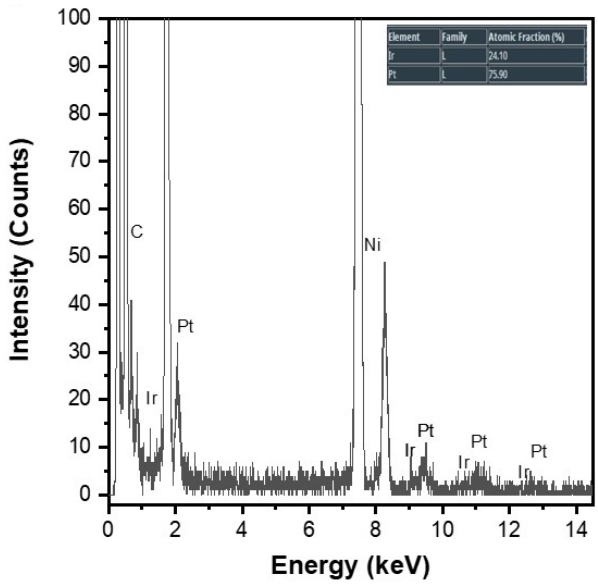

Figure S2. EDS spectra of the PtIr NWs.

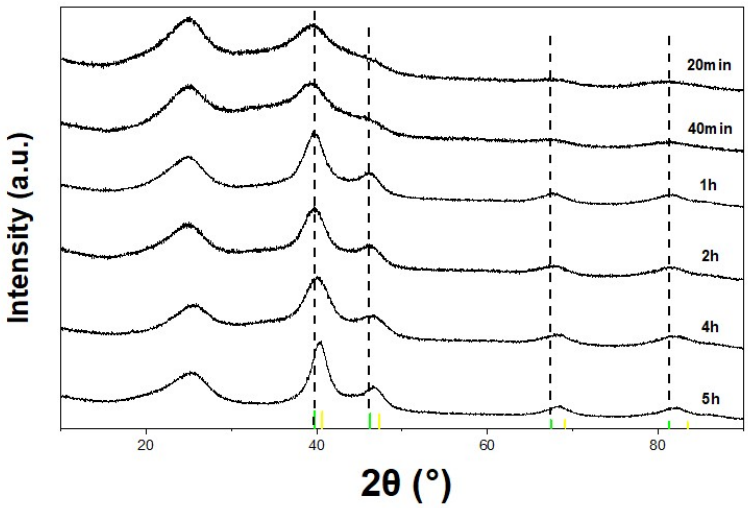

Figure S3. XRD patterns of the products for the PtIr NWs synthesis obtained at reaction times of 20, 40 min and 1, 2, 4 and 5 h.

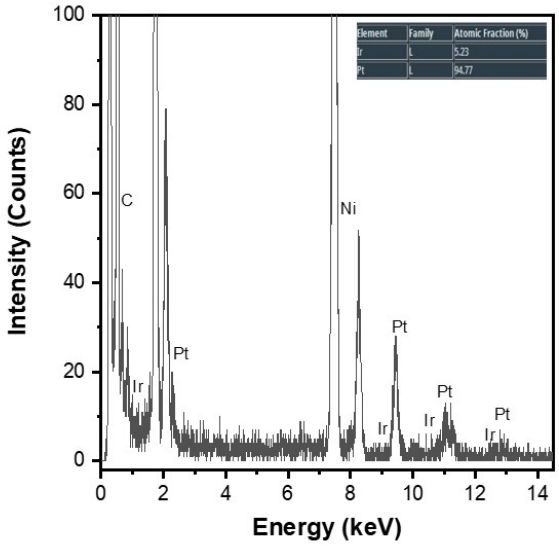

Figure S4. EDS spectra of the PtIr NWs products obtained at 20 min of reaction.

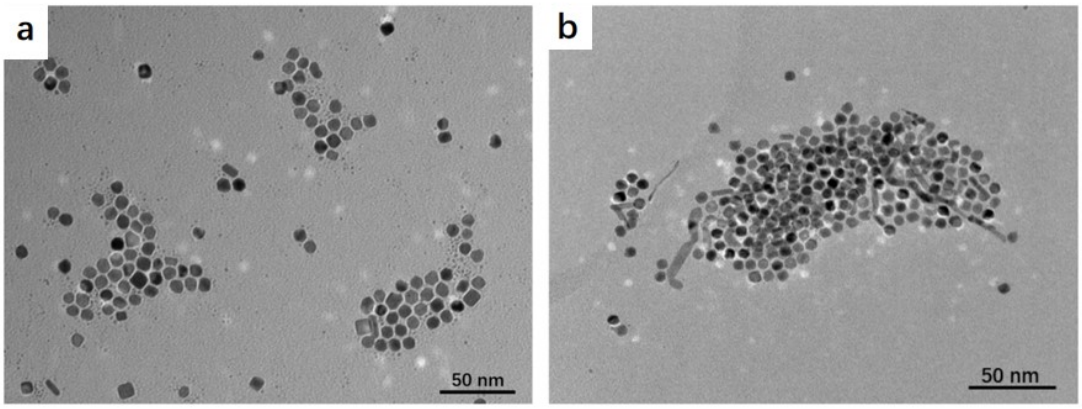

Figure S5. TEM images of products synthesized without adding DDAB. (a) reacted at 170°C for 5 h. (b) reacted at 200℃ for 12 h.

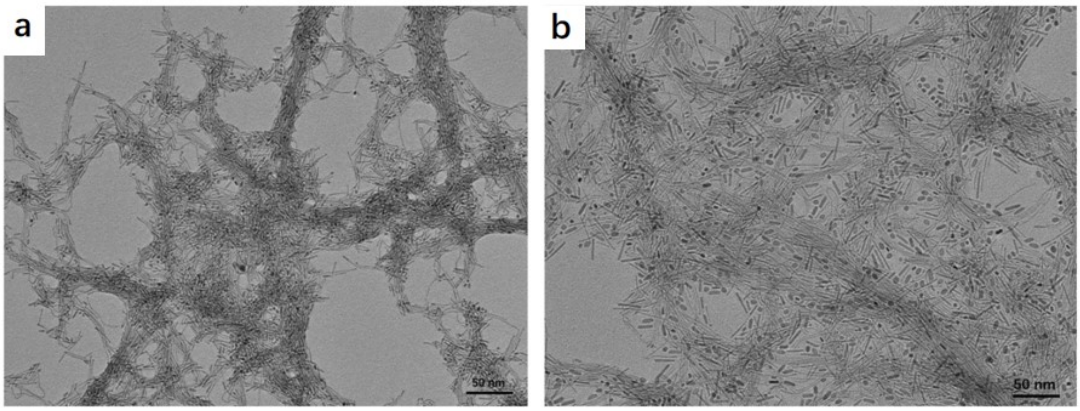

Figure S6. TEM images of products obtained by changing DDAB with (a) DDAC. (b) CTAB.

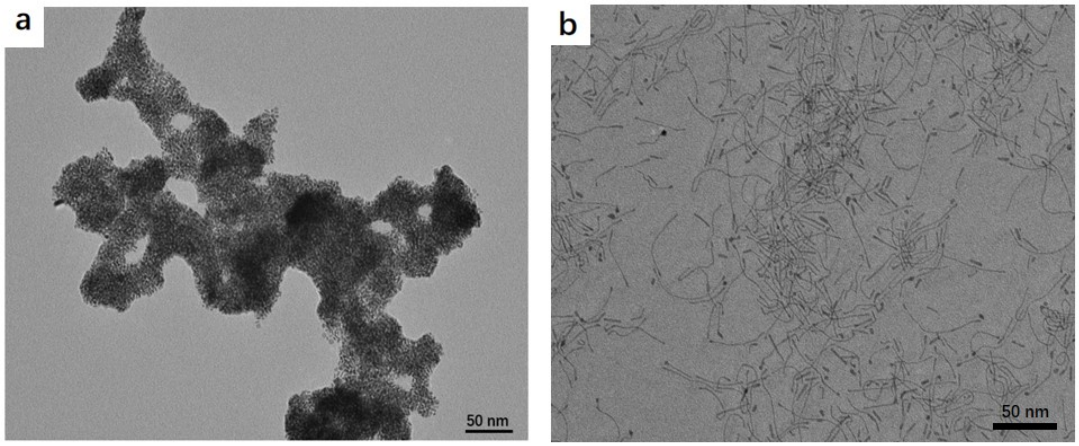

Figure S7. TEM images of products obtained (a) without $W(CO)_6$. (b) with $W(CO)_6$ replaced by $Mo(CO)_6$.

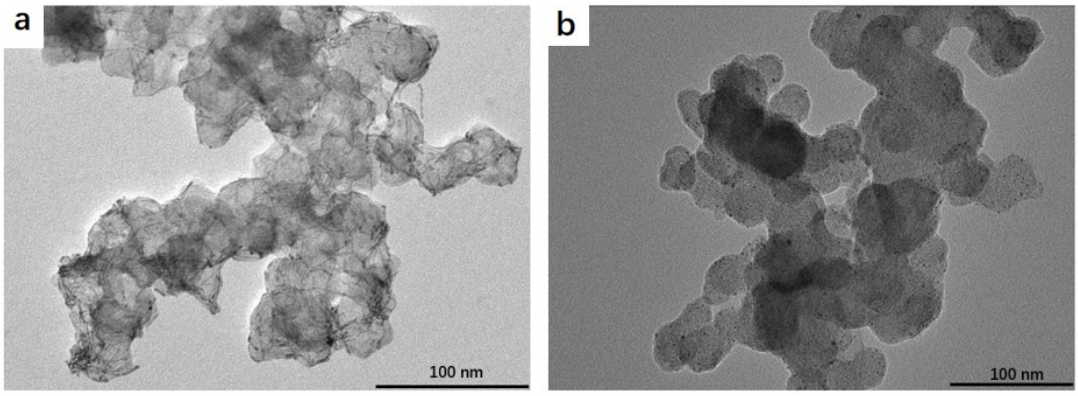

Figure S8. TEM images (a) PtIr NWs supported on carbon. (b) PtIr NPs supported on carbon.

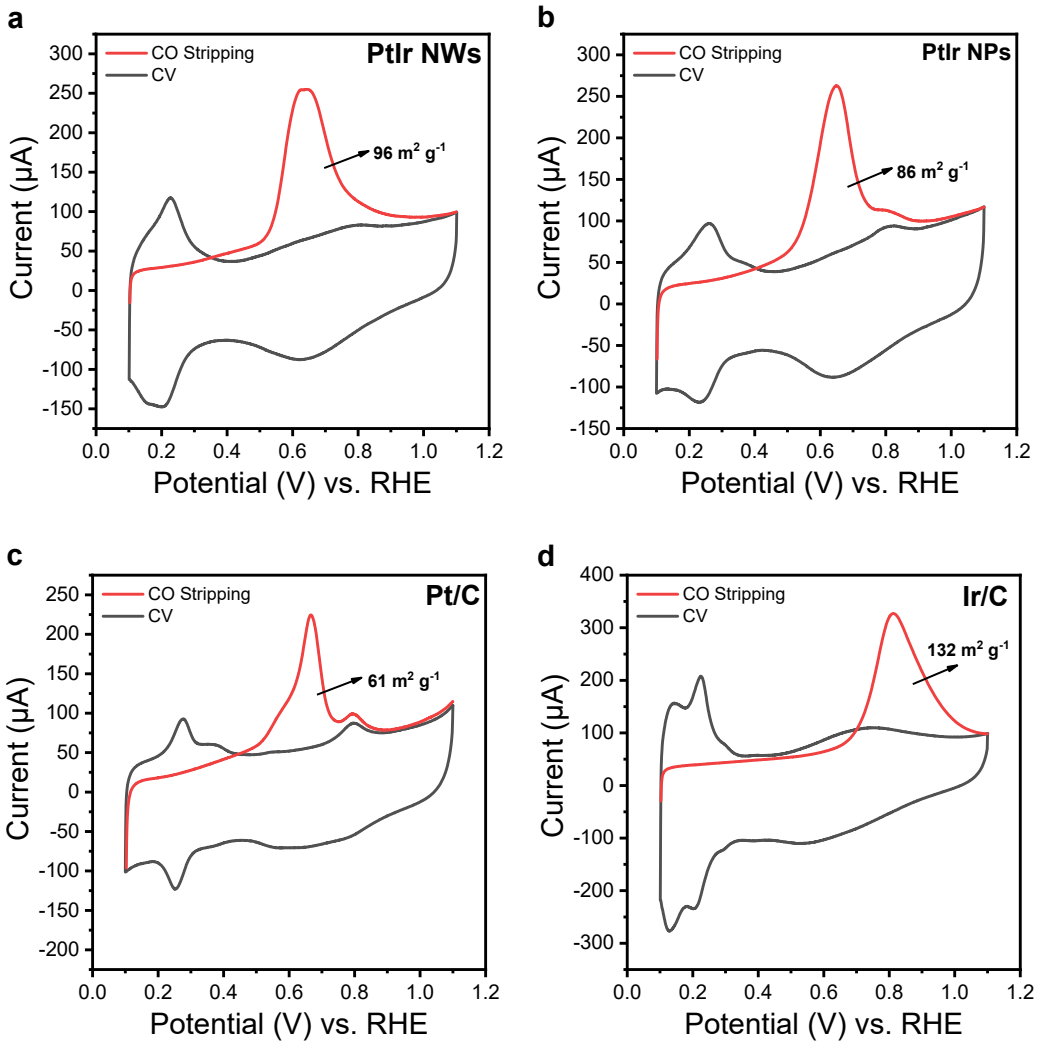

Figure S9 CO stripping tests of (a) PtIr NWs, (b) PtIr NPs, (c) Pt/C and (d) Ir/C. The curves were obtained in 1 M KOH. The electrode was hold at 0.2 V in CO saturated electrolyte for 15 min, and then bubbled with Ar for 20 min to remove the CO residue. Then the electrode was scanned from 0.1 to 1.1 V at 50 mV s^{-1} to obtain the CO stripping curve. The CV curves were obtained in Ar saturated electrolyte at a scan rate of 50 mV s^{-1}. The ECSA was calculated by integrated the transferred charge of the CO oxidation peak using the CV curve as background (i.e., the pointed area) and then normalized by the constant of 420 μC cm^{-2} for a two-electron transfer assuming the oxidation of one CO to CO_2 per PGM atom.

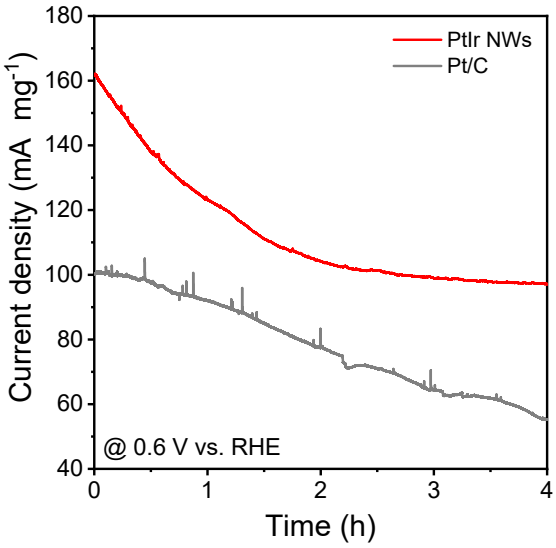

Figure S10 Stability tests of the PtIr NWs and Pt/C for AOR in 1 M KOH + 0.1 NH_3 at 0.6 V.

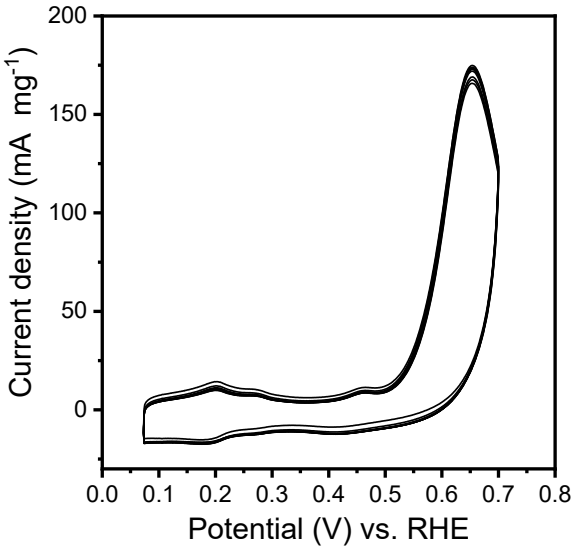

Figure S11 CV curves of the PtIr NWs at a scan rate of 5 mV s^{-1} and a rotation speed of 900 rpm in 1 M KOH + 0.1 M NH_3.

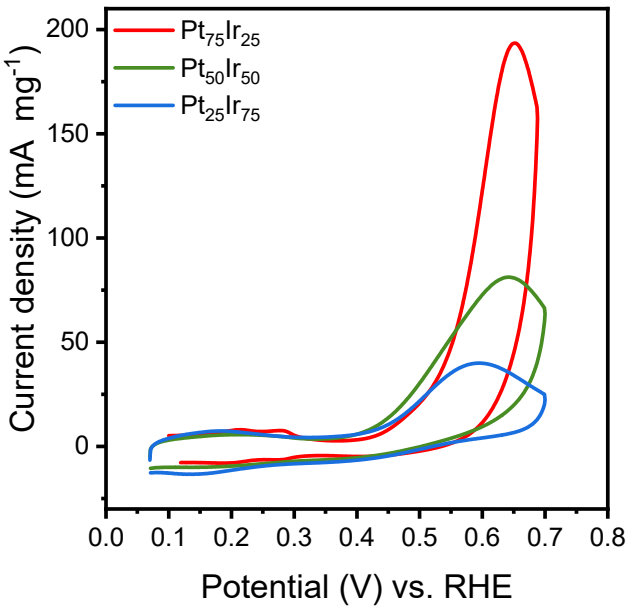

Figure S12. Polarization curves of $Pt_{75}Ir_{25}$, $Pt_{50}Ir_{50}$, and $Pt_{25}Ir_{75}$ in 1 M KOH + 0.1 M NH_3. The curves are obtained at a scan rate of 10 mV s^{-1} and a rotation speed of 1600 rpm.

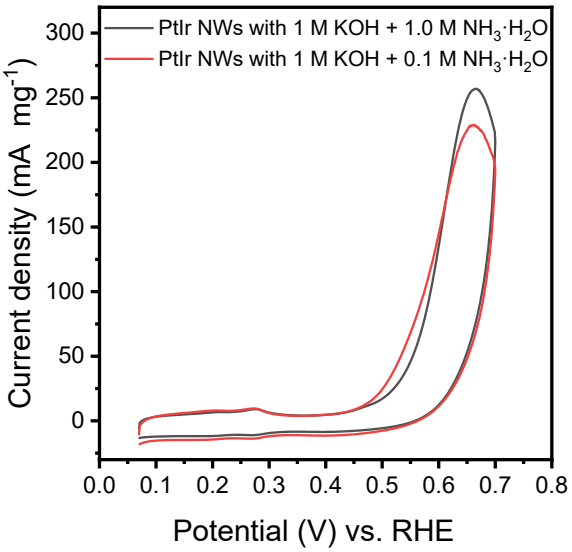

Figure S13 Polarization curves of PtIr NWs tested in 1 M KOH with 0.1 M NH_3 or 1.0 M NH_3 at a scan rate of 10 mV s^{-1} and a rotation speed of 1600 rpm.

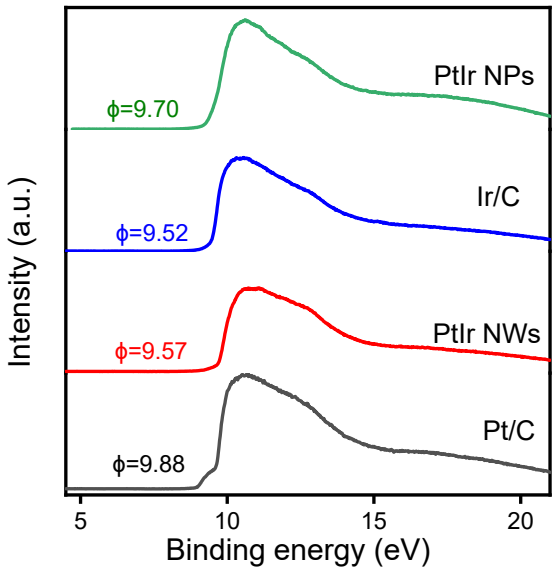

Figure S14 UPS spectra of PtIr NWs, PtIr NPs, Ir/C and Pt/C

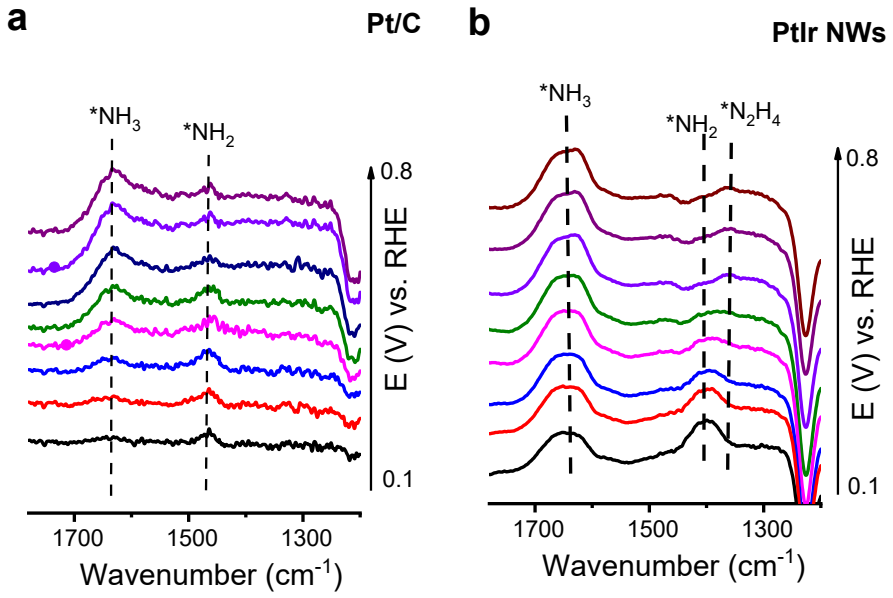

Figure S15 In situ electrochemical ATR-SEIRAS spectra of (a) Pt/C and (b) PtIr NWs.

Table S1. Summary of the AOR activities.

Catalyst	ECSA ($m^2\ g^{-1}$)	Onset potential (mV)	Tafel slope ($mV\ dec^{-1}$)	Mass activity at 0.6V ($mA\ mg^{-1}$)	Specific activity at 0.6V ($mA\ cm_{ECSA}^{-2}$)
PtIr NWs	88	405	121	124	0.141
PtIr NPs	63	435	125	77	0.122
Pt/C	55	512	91	54	0.097
Ir/C	123	392	324	20	0.016

Table S2. Summary of the AOR activities of the Pt-based catalysts.

Catalysts	Electrolyte	Onest potential (V vs. RHE)	Mass activity at 0.6 V ($mA \bullet mg_{PGM}^{-1}$)	Specific activity at 0.6 V ($mA \cdot cm_{ECSA}^{-2}$)	Ref.
PtIr NWs	1 M KOH + 0.1 M NH_3	0.405	125	0.72	This work
$Pt_{33}Zn_1$ alloys	1 M KOH + 0.1 M NH_3	0.49	~30	-	S1
PtCoSn/C	1 M KOH + 0.1 M NH_3	0.499	~175	-	S2
Pt_7Co_2-N-C	1 M KOH + 0.1 M NH_3	0.4	~35	-	S3
High-entropy PtRuFeCoNi nanoalloys	1 M KOH + 0.1 M NH_3	0.42	~70	-	S4
PtFeCoNiIr/C	1 M KOH + 0.1 M NH_3	0.389	~95	-	S5
Bead-like Pt	1 M KOH + 0.1 M NH_3	0.42	-	~1.2	S6
$Ni_7Pt_{86}Mo_7$ Alloy	1 M KOH + 0.1 M NH_3	0.49	~55	-	S7
Pt_7Ir_3 NPs	1 M KOH + 0.1 M NH_3	0.39	~35	-	S8
PtIrCu	1 M KOH + 0.1 M NH_3	0.37	102	-	S9
Pt/TiO_2/S-OLCN	1 M KOH + 0.1 M NH_3	-	-	0.36	S10

Reference

[S1] Z. Tao, H. Yu, S. Li, W. Xia, C. Wang, X. Liu, S. Zhang, J. Ma, X. Zhu, M. Ge, S. Liu and X. Yuan, *ACS Sustainable Chemistry & Engineering*, 2026, **14**, 2073-2082.

[S2] C. Dai, X. Yuan, Y. Wang, X. Liu, C. Ju, L. Hu, S. He, R. Shi, Y. Liu, J. Zhang, Y. Zhu and J. Wang, *Small*, 2025, **21**, 2501582.

[S3] F. Fang, Q. Cheng, M. Wang, Y. He, Y. Huan, S. Liu, T. Qian, C. Yan and J. Lu, *ACS Nano*, 2025, **19**, 1260-1270.

[S4] T. Hu, Z. Zhang, S. Wang, Y. Wang, J. Yang and Y. Li, *Journal of Electroanalytical Chemistry*, 2025, **995**, 119302.

[S5] Y. Zhang, Z. Wang, L. Wang and L. Zong, *Small*, 2024, **20**, 2400892.

[S6] H. Tang, Y. Gu, J. Luo, W. Zhang, J. Zhang and Y. Zhou, *ChemistrySelect*, 2024, **9**, e202400482.

[S7] S. Liu, Y. Jiang, M. Wang, Y. Huan, Y. He, Q. Cheng, Y. Cheng, J. Liu, X. Zhou, T. Qian and C. Yan, *Advanced Functional Materials*, 2023, **33**, 2306204.

[S8] H. Fang, C. Liao, Q. Cai, F. Zhong, L. Lin, C. Chen, Y. Luo and L. Jiang, *Chemical Engineering Science*, 2023, **280**, 118836.

[S9] H. Yang, X. Huang, Z. Liu, X. Lin, Q. Chen, J. Li, C. Zhang, Z. Peng Kan, Z. Qun Tian and P. Kang Shen, *Journal of Colloid and Interface Science*, 2023, **652**, 1764-1774.

[S10] L. L. Sikeyi, L. R. Bila, T. D. Ntuli, C. T. Selepe, N. W. Maxakato, N. J. Coville and M. S. Maubane-Nkadimeng, *Diamond and Related Materials*, 2023, **132**, 109612.